Transient Electric Birefringence of Segmentally Flexible Macromolecules in Electric Fields of Arbitrary Strength

ARTICLE *in* THE JOURNAL OF PHYSICAL CHEMISTRY B · DECEMBER 2000

Impact Factor: 3.3 · DOI: 10.1021/jp0018100

4 AUTHORS, INCLUDING:

F. Guillermo Díaz Baños
University of Murcia
47 PUBLICATIONS **472** CITATIONS
SEE PROFILE

José García de la Torre
University of Murcia
217 PUBLICATIONS **6,099** CITATIONS
SEE PROFILE

Transient Electric Birefringence of Segmentally Flexible Macromolecules in Electric Fields of Arbitrary Strength

F. G. Díaz, B. Carrasco, M. C. López Martínez, and J. García de la Torre*

Departamento de Química Física, Universidad de Murcia, 30071 Murcia, Spain

Received: May 17, 2000; In Final Form: September 28, 2000

We study in this work the decay of the electric birefringence from the steady-state value to zero when an orienting electric field applied on a macromolecule is switched off. We consider specifically the case of segmentally flexible macromolecule with only two subunits and one hinge. Using Brownian dynamics as the predicting tool for the dynamics of the molecule, we have paid special attention to important aspects such as hydrodynamic interaction, field strength, and orienting mechanism. Improving statistics to obtain data with very good signal-to-noise ratio, we have found a different behavior of the induced and permanent dipoles in the relaxation process: the first one can be described independently of the intensity of the field while the second shows a dependence of the field strength. Moreover, the time spectrum shows no dependence on the type of dipole or the field intensity, and amplitudes appear to be essential in characterizing the relaxation of the molecule. According to our results, hydrodynamic interaction could be very important in describing the relaxation times of a molecule, but amplitudes are not affected by this refinement, which should be a very interesting advantage for the application and development of different simplified theories.

Introduction

The time dependence of the effects produced in a macromolecule in solution by an external agent, such as an electric field, contains valuable information about the macromolecule. An important case in this regard is the transient birefringence or dichroism caused by an electric field.[1−4] For a rigid macromolecule, the kinetics of the rise or decay of the birefringence, caused by the reorientation of the particle, depends essentially on the rotational diffusivity of the rigid particle, determined by the three eigenvalues of its rotational diffusion tensor.[5,6]

For flexible macromolecules, the situation is even more complex, interesting, and informative. The reorientation of the individual units comprising the macromolecule necessarily causes a change in the macromolecular conformation, and the kinetics of such changes depends not only on the overall size and shape, as in the case of the rigid particle, but also on the internal structure, i.e., on the kind and degree of flexibility of the macromolecule. Furthermore, the type and strength of the molecule−field interactions are intricately interwoven with flexibility and hydrodynamics in the determination of the rate of the transients. Therefore, important information on electrooptical properties is also contained in the transients. In a number of cases, flexibility is distributed across the whole macromolecule. Such is the case for double-helical DNA, described by the well-known wormlike model.[7] Transient electric birefringence has been employed to detect the flexibility of DNA in a number of studies (for instance, see refs 8−10).

Flexibility is neatly localized at some small regions in another kind of semiflexible macromolecule. It is said that those macromolecules are segmentally flexible,[11] because they are constituted by a few rigid subunits linked by means of semiflexible hinges or swivels. A preceding paper from our group[12] (where references to the literature of segmentally flexible macromolecules can be found) has been devoted to the problem of orientation and deformation of macromolecules of this type. Those effects can be detected by light scattering as well as by birefringence, and can be caused not only by electric fields, but also by other external agents such as flows. In that work,[12] we have treated the case of the steady-state properties reached by the macromolecule when it has been subjected to the external agent for a sufficiently long time. In the present work, we consider the dynamics of this process, i.e., the rate of the approach to the equilibrium.

Particularly, we study here the decay of the electric birefringence (or dichroism) from the steady-state value to zero, when the field is switched off. This process is easier to study experimentally and theoretically than the birefringence rise. For segmentally flexible macromolecules, the rate of the electric birefringence decay is expected to be a sensitive manifestation of the flexibility. Indeed, this experimental technique has been used to probe segmental flexibility in several cases of great biological interest, such as the four-subunit muscle molecule, myosin.[7,13,14] We consider specifically the case of segmentally flexible macromolecules with only two subunits and one hinge. This case has theoretical interest, since it is the simplest one that includes internal flexibility and motion, and is also of practical applicability to, for instance, two-subunit fragments of the myosin molecule.[15] In addition, the more general trends and conclusions found for this case might be useful guidelines for other cases.

An aspect that will be regarded with special interest is the effect of field strength. Traditionally, electric birefringence decay experiments have been done with weak fields, first to avoid sample alterations, but also to analyze the results in terms of theoretical treatments that are easier or even only exist for very weak fields. Furthermore, under such conditions one probes the dynamics of an unperturbed molecule. However, the possibility of using strong fields is very interesting. As is known for rigid

* To whom correspondence should be addressed.

10.1021/jp0018100 CCC: $19.00
Published on Web 12/05/2000

macromolecules,[16−19] the time dependence of birefringence depends and supplies information on electrical properties of the molecule and the molecule−field interaction mechanism. For semiflexible macromolecules, the ability of the particle to deform in an intense field[12] implies that the field-off decay of properties will manifest the relaxation of such deformation. Hints of this fact have been manifested in electric dichroism experiments on DNA in some atypical electrooptic transients[20] and by simulation.[21,22]

Another aspect treated carefully will be the influence of the different types of orienting mechanism in the decay process. Wegener[23] made a complete analytical description of the transient electric birefringence at low field strengths for completely rigid models. In flexible models, the induced dipole has received more attention,[24,25] although some recent experiments have been performed with molecules showing permanent dipoles[26] or assuming in the interpretation of data that the birefringence decay times are independent of the nature of the orienting forces for sufficiently low fields.[27] In some other cases the assumption has been made that both permanent and induced dipole orienting mechanisms result in essentially identical decay behavior for relatively low fields.[28] Allison and Nambi[25] also studied the saturation-induced dipole orienting mechanism, which could be thought to be equivalent to a permanent dipole.

On the theoretical side, a comprehensive, general and yet simple description of the dynamics of segmental semiflexibility seems unfeasible, and the electrooptics transients add even more complexity. Only some particular aspects of the problem have been theoretically developed, usually making approximations or assumptions that limit the validity or applicability of those treatments (vide infra). Thus, some works neglect hydrodynamic interactions, assume low-field behavior, or consider only a part of the transient (for a review on the dynamics of segmental flexibility, see ref 29). One of the points which has not received much attention is the calculation of amplitudes associated to each relaxation time. We are going to study the characterization of the system through these very sensitive parameters.

In the present work, the tool for predicting the dynamics of birefringence decay is Brownian dynamics simulation. In the study of dynamic properties a Brownian trajectory can be simulated from the first principles of Brownian motion. A number of examples of the applicability of the Brownian dynamics simulation (BD) technique for macromolecules under the influence of external forces are available in the recent literature, including individual chains in flows[30−32] and fields.[33,34] The technique has already been used for segmentally flexible macromolecules[30,35−38] and wormlike macromolecules.[21,22,39] The above-mentioned important aspects such as hydrodynamic interactions, field strength, etc., can be included in the BD simulation algorithms in a quite rigorous manner; this simulation technique is a powerful tool to investigate their effects.

From Brownian trajectories, birefringence decay profiles will be analyzed, and some observations regarding the robustness of the sensitivity of decay lifetimes and amplitudes on noise will be made. Although this is not a serious problem when simulating equilibrium fluctuations, such as the intensity autocorrelation function in dynamic light scattering, because many sampling points occur in a given trajectory, this is a relevant problem for transient phenomena.

Theory, Model, and Methods

Model. We consider a segmentally flexible macromolecule composed of two rigid subunits ("arms") joined by a semiflexible swivel, interacting with an electric field. The mechanical and electrooptical description of the model is as described in our preceding paper.[12] We just summarize here the main features. The potential energy of a given configuration of the model in the field has two terms, one associated with bending and other due with the interaction with the field. The bending potential is

$$\frac{V_{\text{elect}}}{k_{\text{B}}T} = Q(\alpha - \alpha_0)^2 \tag{1}$$

where α_0 is the equilibrium value of the angle defined by the subunit axes ($\alpha_0 = 0$ for fully extended, straight conformation) and Q is the flexibility parameter, with $Q = 0$ for the completely flexible case and $Q \rightarrow \infty$ for the completely rigid one.

The interaction between the molecule and the field arises from permanent or induced dipoles. The corresponding potential energy is given by

$$\frac{V_{\text{elect}}}{k_{\text{B}}T} = -\sum_{i=1}^{2}(a_i \cos\theta_i + b_i \cos^2\theta_i) \tag{2}$$

where $\cos\theta_i = (\mathbf{E}\cdot\mathbf{u}_i)/E$ is the cosine of the angle between the electric field $\mathbf{E}$ and the arm vector $\mathbf{u}_i$. The electric parameters are $b_i = 0$ for a purely permanent dipole moment and $a_i = 0$ for a purely induced moment (IND). In the case of permanent dipoles, we consider two possibilities: for dipoles joined head-to-head (PHH), a_1 and a_2 are positive, while for the head-to-tail case (PHT) we take a_1 positive and a_2 negative. The field intensity, or, more precisely, the strength of the molecule−field interaction, is governed by the values of a's and b's, a being proportional to E and b proportional to E^2.

At a certain instant of time, t, the excess birefringence of a macromolecular solution with respect to that of the pure solvent, $\Delta n(t)$, is an ensemble average over the values contributed by each molecule in the sample. The individual, instantaneous value has in turn two contributions, one from each arm in the two-subunit macromolecule. Thus, $\Delta n(t)$ can be written as

$$\Delta n(t) = C(x_1\langle P_2(\cos\theta_1)\rangle + x_2\langle P_2(\cos\theta_2)\rangle) \tag{3}$$

where $P_2(\cos\theta_i) = (3\cos^2\theta_i - 1)/2$. In eq 3, the fractions x_1 and x_2 (with $x_1 + x_2 = 1$) are proportional to the optical polarizabilities, $(\gamma_{\parallel} - \gamma_{\perp})_i$, of the subunits. Although the treatment can be carried out for different subunits, all the results to be presented here will be for two identical subunits, so that $x_1 = x_2 = 1/2$. C in eq 3 represents a constant characteristic of the material, but independent of conformation, field intensity, etc. This constant does not have to be specified if we normalize the time-dependent birefringence, $\Delta n(t)$, to the saturation value, Δn_{sat}; thus

$$\Delta n(t)/\Delta n_{\text{sat}} = \Delta n'(t) = (1/2)(\langle P_2(\cos\theta_1)\rangle + \langle P_2(\cos\theta_2)\rangle) \tag{4}$$

Another way of expressing the results is to normalized to the zero time value $\Delta n(0)$, with $t = 0$ when the field is switched-off:

$$\Delta n^*(t) = \frac{\Delta n(t)}{\Delta n(0)} = \frac{\Delta n'(t)}{\Delta n'(0)} \tag{5}$$

Unless we say the opposite, we shall use the normalization given by eq 5. For a more detailed description, the reader is referred to our preceding paper.[12]

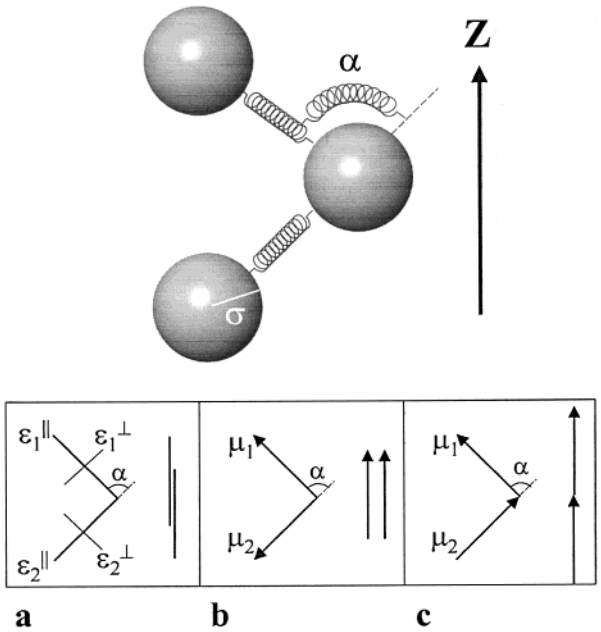

Figure 1. Hydrodynamic version of a two-subunit particle: the trumbbell model. Also scheme of the electric properties: (a) electric polarizabilities; (b) permanent dipole moments, head-to-tail disposition; (c) permanent dipole moments, head-to-tail disposition.

In the present work, we have to specify the model further, giving its hydrodynamic features that determine the dynamics of the transient electrooptics. For this purpose, we employ the semiflexible trimer or "trumbbell",[24,40,41] which is depicted in Figure 1. It is composed of three identical beads joined by two quasirigid bonds. The central bead in the trumbbell acts as a semiflexible joint, allowing restricted bending with an associated restoring potential given by eq 1. The bonds are stiff springs with equilibrium length b and a spring constant such that the mean squared length when no external forces are present is $1.05b^2$. Previous Brownian dynamics simulation studies have been reported by these authors,[30,35,36,38] where more details about this model can be found.

In the same way that eq 5 gives a normalized value for birefringence, it is useful to use dimensionless variables and parameters in both the simulation procedure and the presentation of results. Therefore, lengths and distances are expressed in dimensionless form by dividing them by the spring length, b; forces are divided by kT/b and time is normalized multiplying by $kT/\zeta b^2$, where $\zeta = 6\pi\eta_0\sigma$, where η_0 is the solvent viscosity and σ is the bead radius. All dimensionless quantities are hereafter denoted by an asterisk.

Brownian Dynamics Simulation. We use a simulation procedure based on the algorithm of Ermak and McCammon,[42] with a modification proposed by Iniesta and García de la Torre.[43] Each step is taken twice, in a predictor−corrector manner, and the position of the beads $\mathbf{r}_i$ after the time step, Δt, are obtained from the previous ones, $\mathbf{r}_i^0$, according to

$$\mathbf{r}' = \mathbf{r}^0 + \frac{\Delta t}{kT}\mathbf{D}^0\cdot\mathbf{F}^0 + \Delta t(\nabla_r\mathbf{D})^0 + \mathbf{R}^0 \qquad (6a)$$

$$\mathbf{r} = \mathbf{r}^0 + \frac{\Delta t}{kT}(\mathbf{D}^0\cdot\mathbf{F}^0 + \mathbf{D}'\cdot\mathbf{F}') + \Delta t\frac{1}{2}(\nabla_r\mathbf{D})' + \mathbf{R}' \qquad (6b)$$

Equation 6a is for the predictor substep, which is taken with basis on the quantities corresponding to the initial conformation, $\mathbf{r}^0$, denoted with the 0 superscript. In this step, an estimate, $\mathbf{r}'$, of the final conformation is obtained, and the necessary quantities are evaluated at it. Next the corrector step is taken as indicated in eq 6b, again from the initial conformation, $\mathbf{r}^0$, but using quantities that are the mean of those at $\mathbf{r}^0$ and $\mathbf{r}'$. Although the step in our predictor−corrector procedure is equivalent to two Ermak−McCammon steps and subsequently it takes about twice the CPU time of the latter, longer time steps are allowed.

The $3N$ components of the vector $\mathbf{r}$ are the coordinates, $\mathbf{r}_i$. $\mathbf{D}$ is the $3N \times 3N$ diffusion supermatrix whose ij blocks are the diffusion tensors, $\mathbf{D}_{ij}$. $\mathbf{F}_i$ are the total forces on the N beads and should be the sum of two contributions, the internal forces (spring forces in this case) and the external forces (to quantify the molecule-field interaction). We are interested only in the field-free decay, and due to the procedure of simulation (see below), we do not need to include this second contribution in the Brownian simulations. $\mathbf{R}^0$ and $\mathbf{R}'$ are the random vectors with covariance matrix equal to $2\Delta t\mathbf{D}^0$ and $2\Delta t\mathbf{D}'$, respectively. They are calculated from Gaussianly distributed random vectors of zero mean and unit covariance, $\mathbf{q}$ and $\mathbf{q}'$, as $\mathbf{R}^0 = (2\Delta t\sigma^0\mathbf{q})^{1/2}$ or $\mathbf{R}' = (2\Delta t\sigma'\mathbf{q}')^{1/2}$, where the $3N \times 3N$ matrix σ is obtained from the square root of $\mathbf{D}$.

The ii blocks of the diffusion supermatrix are always given by $\mathbf{D}_{ii} = (kT/\zeta_i)\mathbf{I}$, where $\mathbf{I}$ is the unit 3×3 matrix, ζ_i is the friction coefficient of the bead $\zeta_i = 6\pi\eta_0\sigma$, where η_0 is the viscosity of the solvent. For the simulation of the dynamic properties, the hydrodynamic interaction (HI) between beads must be properly accounted for. We accomplish this using the Rotne−Prager−Yamakawa modification of the Oseen tensor,[44,45] which corrects for the nonpointlike nature of the frictional elements and describes correctly the possibility of overlapping (of equal-sized beads). Thus, we include HI setting $\mathbf{D}_{ij} = kT\mathbf{T}_{ij}$, where $\mathbf{T}_{ij}$ is the above-mentioned tensor.

Birefringence Decay Functions and Fittings. Using the Brownian dynamics algorithm, individual trajectories are simulated for a large number of molecules. We consider that molecules do not interact hydrodynamically (or in any other sense) with each other, so the trajectory simulated for each molecule is independent of the rest. At any given time, $P_2(\cos\theta_1)$ and $P_2(\cos\theta_2)$ are evaluated for each molecule, and from their sample averages, the birefringence is calculated from eq 4. In a typical simulation, the initial conformations of the molecules in the sample correspond to absence of field, and are generated with the conformational statistics determined by V_{int} (eq 1). Then the electric field is applied, and the simulation proceeds for a time that is sufficiently long so that steady-state birefringence is clearly reached. At some given instant, the field is switched off and the simulation is continued, so that the decay of the birefringence is monitored. The duration of the decay is sufficiently long so that the final birefringence is zero within statistical error.

In the present study we regard, exclusively, the birefringence decay for the reasons mentioned above. Therefore, the field-on, birefringence-rise first part of the simulation, which has to be long to make sure that the steady state is reached, is somehow useless for our purposes. To save computing time, alternative strategies can be employed. One of them consists of simulating the rise part of the trajectory without hydrodynamic interactions, which is computationally less expensive. This affects the rise kinetics, which is not considered here, but the steady state reached is the same. Another possibility consists of starting the simulation with a sample of molecules generated in the presence of field, generated with the Monte Carlo procedure described in our previous work on steady-state properties.[12] Either of the two procedures is useful for the present work, as we are just interested in the field-off decay of birefringence.

The resulting time decay series can be fitted to a sum of exponentials

$$\Delta n^*(t) = y(t) = a_1 e^{-t/\tau_1} + a_2 e^{-t/\tau_2} + ... \quad (7)$$

Due to normalization, the $y(t)$ functions decay from $y(0) = 1$ to $y(\infty) = 0$, so in this case $a_1 + a_2 + ... = 1$.

As described below, from theoretical grounds one may expect that this time function is a sum of exponentials. In any case, it is useful to have the decays fitted to a multiexponential for further numerical work.

The fitted relaxation times and amplitudes are indexed as (τ_1,a_1), (τ_2,a_2), ... We adopt the convention that τ_1 is the longest relaxation time. For the multiexponential fit, we have employed the commercial program Sigmaplot.[46] In a previous study, based on the fitting of several simulations (results not shown), we have checked that this procedure yields the same results as the well-known DISCRETE program, written by Provencher[47,48] for a discrete sum of exponentials.

Following a practice common with other properties, particularly dynamic light scattering, relaxation constants can be defined[19,49] that describe the mean rate of the birefringence decay and the rate at the initial instant. The integral over t of the normalized birefringence decay is a characteristic time that represents the mean relaxation rate over the whole time range, given by

$$\tau_{mean} = \int_0^\infty y(t)\, dt \quad (8)$$

The initial decay rate can be expressed in terms of a quantity similar to the first cumulant in dynamic scattering. We define

$$1/\tau_{ini} \equiv b_{ini} \equiv -\left(\frac{d \ln y(t)}{dt}\right)_{t=0} \quad (9)$$

b_{ini} is the initial slope of the decay. If the time dependent birefringence decay function is expressed as a sum of exponentials, as in eq 7, then it follows that

$$\tau_{mean} = a_1\tau_1 + a_2\tau_2 + ... \quad (10)$$

and

$$1/\tau_{ini} = a_1/\tau_1 + a_2/\tau_2 + ... \quad (11)$$

An important feature of τ_{ini} and τ_{mean} is that they are more robustly fitted parameters than the individual relaxation times τ_1, τ_2, ... (their values are more stable and present less statistical error).

Results and Discussion

Simulation Conditions. We have studied the relaxation process of Δn, paying attention to both the influence of the intensity of the orienting field and its dependence on the different orienting mechanisms. Despite the simplicity of the three-bead model used to represent molecules possessing central bends, we think that the conclusions obtained can be extended to models consisting of more beads.

For that purpose we have simulated the birefringence decay for two extreme cases of the field strength: very low and infinitely high. In experimental work, the study of birefringence dynamics at very high (saturating) fields is uncommon because of problems about instrumentation, sample alterations, or data interpretation. However, the prediction of the behavior under such conditions represents one limiting, but very illustrative, situation in the study of field strength effects. In addition, the simulation of birefringence decay is particularly easy, since the previous step of obtaining the initial conformation is not necessary (see below), and the signal-to-noise ratio of the results is optimum.

The simulation of birefringence decay, for molecules with two arms, from an infinitely strong field is started from a sample of molecules that are perfectly aligned with the field. Three cases are possible in this regard:

1. For permanent dipoles joined head-to-tail (PHT), both arms must be aligned with the field, pointing in the same direction. This implies that, regardless of the values of Q and α_0, all the molecules have initially $\alpha = 0$ (the arms are open; see Figure 1c).

2. For permanent dipoles joined head-to-head (PHH), the same restrictions apply, but the effect on macromolecular conformation is the opposite: now, all the molecules have initially $\alpha = 180°$ (the arms are closed; see Figure 1b).

3. For induced dipoles (IND), both arms must be aligned with the field, but they can point either upward or downward (see Figure 1a). There are now two possible conformations: A, with $\alpha = 0$, and B, with $\alpha = 180°$. The ratio (head-to-head/head-to-tail) of their probabilities is $e^{-Q\pi^2}$.

For molecules immersed in a weak field a characteristic group of initial conformations is obtained through Monte Carlo simulation. The three cases mentioned above should be the limiting configurations.

In our simulations, the time step has been always $\Delta t^* = 5 \times 10^4$; $\alpha_0 = 0$ and the radii of the spheres $= 0.5$. Flexibility ranges from $Q = 0$ (total flexibility, unrestricted bending) to $Q = 50$ (practically rigid) with an intermediate value of $Q = 0.5$. To be certain that the molecules have had time enough to relax completely, each trajectory has been given 3 units of time.

After each simulation, the resulting decay data were submitted to multiexponential analysis as described above, obtaining the amplitudes, relaxation constants (eq 7), and the initial and mean rates (eqs 10 and 11). Fitting results for the permanent head-to-tail model are shown in Table 1. The values of the different parameters obtained for the induced model are presented in Table 2, where data from Roitman and Zimm[24,41] can also be found. Some examples of the decay of $\Delta n^*(t)$ are displayed in Figures 2−4. The scale of the $\Delta n^*(t)$ axis is chosen as linear or logarithmic, depending on the feature of the curve that is most relevant. Note that in the decay from very high fields birefringence is initially saturated, so that $\Delta n^*(0) = 1$. In the rest of the cases the values have been normalized to the one at $t = 0$.

Some remarks about the procedure of fitting must be added. To obtain good fittings, the number of trajectories needs to be large. The reason is that, in addition to the intrinsic difficulty of the multiexponential fitting, there are three factors that influence the statistical quality of the data: intensity of the field, flexibility of the model, and hydrodynamic interaction. The problem is that uncertainty can mask the decay spectrum. This means that very good statistics are needed. In fact, results could mislead us very easily. Consequently, it is important to evaluate the quality of our numerical results. The criterion we have applied is reproducibility. For that purpose, we have increased the number of molecules until the results of the fitting for all the independent simulations under certain given conditions could be compared within a reasonable statistical uncertainty. Finally we have found that eight independent simulations of 250 000 molecules for the best conditions (no HI, very low flexibility, and high field) and four independent simulations of 4 000 000

TABLE 1: Relaxation Times and Amplitudes for the PHT Model

Q	a_i	a_1	τ_1	a_2	τ_2	a_3	τ_3	τ_{ini}	τ_{mean}	$\Delta n(0)$
					no HI					
0.0	1	0.853	0.182	0.147	0.052			0.099	0.162	0.061
	∞	0.504 ± 0.030	0.192 ± 0.004	0.427 ± 0.022	0.082 ± 0.005	0.069 ± 0.010	0.016 ± 0.002	0.079	0.133	1.000
0.5	1	0.925 ± 0.003	0.248 ± 0.001	0.073 ± 0.003	0.035 ± 0.002			0.134	0.232	0.106
	∞	0.675 ± 0.015	0.252 ± 0.003	0.253 ± 0.010	0.057 ± 0.007	0.072 ± 0.024	0.014 ± 0.003	0.079	0.186	1.000
50	1	1.000 ± 0.002	0.346 ± 0.003					0.287	0.347	0.194
	∞	0.999 ± 0.003	0.344 ± 0.001					0.081	0.344	1.000
					HI					
0.0	1	0.833	0.269	0.167	0.099			0.183	0.241	0.061
	∞	0.490 ± 0.048	0.281 ± 0.009	0.436 ± 0.029	0.130 ± 0.011	0.074 ± 0.022	0.047 ± 0.006	0.141	0.198	1.000
0.5	1	0.902 ± 0.020	0.338 ± 0.003	0.095 ± 0.020	0.088 ± 0.032			0.225	0.314	0.106
	∞	0.672 ± 0.008	0.337 ± 0.002	0.259 ± 0.012	0.095 ± 0.006	0.068 ± 0.019	0.035 ± 0.004	0.141	0.253	1.000
50	1	1.000 ± 0.001	0.431 ± 0.002					0.385	0.421	0.193
	∞	0.987 ± 0.002	0.434 ± 0.001					0.146	0.428	1.000

[a] Results obtained from the multiexponential fitting of the decay profiles obtained from simulation.

TABLE 2: Relaxation Times and Amplitudes for the IND Model[a]

Q	b_i	a_1	τ_1	a_2	τ_2	a_3	τ_3	τ_{ini}	τ_{mean}	$\Delta n(0)$
					no HI					
0.0	0.5	0.296	0.172	0.701	0.076			0.085	0.104	0.069
	∞	0.178 ± 0.025	0.200 ± 0.011	0.793 ± 0.023	0.086 ± 0.002	0.028 ± 0.003	0.014 ± 0.001	0.081	0.104	1.000
	RZ	0.219	0.184	0.763	0.080			0.093	0.101	Norm
0.5	0.5	0.684 ± 0.026	0.252 ± 0.007	0.302 ± 0.026	0.055 ± 0.005			0.101	0.189	0.076
	∞	0.672 ± 0.007	0.251 ± 0.002	0.258 ± 0.006	0.057 ± 0.003	0.070 ± 0.012	0.014 ± 0.002	0.081	0.184	1.000
	RZ	0.672	0.239	0.297	0.058			0.126	0.178	Norm
50	0.5	0.984 ± 0.006	0.352 ± 0.002					0.291	0.346	0.554
	∞	0.988 ± 0.004	0.348 ± 0.001					0.079	0.344	1.000
($Z = 5$)	RZ	0.991	0.319	0.005	0.009			0.273	0.316	Norm
					HI					
0.0	0.5	0.199	0.305	0.798	0.141			0.136	0.173	0.069
	∞	0.180 ± 0.060	0.293 ± 0.030	0.743 ± 0.040	0.157 ± 0.007	0.077 ± 0.023	0.060 ± 0.007	0.147	0.174	1.000
0.5	0.5	0.672 ± 0.007	0.337 ± 0.002	0.315 ± 0.007	0.104 ± 0.002			0.164	0.259	0.076
	∞	0.669 ± 0.012	0.336 ± 0.003	0.248 ± 0.012	0.099 ± 0.008	0.083 ± 0.023	0.039 ± 0.005	0.147	0.253	1.000
50	0.5	0.993 ± 0.003	0.432 ± 0.001					0.404	0.429	0.552
	∞	0.986 ± 0.003	0.437 ± 0.001					0.145	0.431	1.000

[a] Results obtained from the multiexponential fitting of the decay profiles obtained from simulation. Results obtained by Roitman and Zimm (RZ) are also included.

for the worst ones (HI, high flexibility, and low field) are reasonable choices. An especially difficult situation is that of total flexibility and very low field. In this case, trying to improve the signal-to-noise ratio, we have preferred to lose information about the standard deviation, but to fit one single decay profile of as many molecules as possible (16×10^6). For each simulation, fitting results are obtained, and from them, averages and standard deviations are obtained. These are the values shown in Tables 1 and 2.

Despite our effort to improve the statistical quality of the data, the spectrum decay obtained from the fitting of the decay profiles must be analyzed very carefully. One extreme example is shown in Figure 2, where we illustrate, for induced dipole and total flexibility, the influence of the intensity of the field in the relaxation process. In the two decay profiles, we can observe that the two initial decades are nearly identical. This is a very strong indication that the relaxation behavior is the same. On the other hand, the fitting procedure detects three exponentials in one case (high field) and only two exponentials in the other (low field). The only difference between both data appears in the last part of the decay. This part, in which the uncertainty of the points is very high, should not be significant, but the fact is that in this case it appears to be important for the fitting of the data. Consequently, although the fitting results (Table 2) show certain differences in the longest relaxation times and their amplitudes, they must not mislead us from the conclusion that, for induced dipoles, the relaxation behavior is independent of field strength. Figure 3 shows a different situation (PHT, total flexibility) in which, despite high uncertainties for low field decay, differences and coincidences between low and high field can be clearly detected and are reflected in the fitting results shown in Table 1.

As a summary, we can say that for the same conditions some results change significantly from one simulation to another, unless the number of molecules is high enough. The main problem is that statistical noise increases when the decay profile reaches low values, but we have noticed that in some cases this region is very important for obtaining reliable values for exponential and preexponential terms in the fitting of the complete relaxation curve. The problem is enhanced at low fields and when flexibility increases. We think that this fact should be taken into account not only in simulations but also in experiments.

Discussion of the Results. *Two different behaviors can be observed for the permanent dipole orientation mechanism (Figure 4).* In the case of very strong field, the initial decay of curves for PHH dipoles is extremely fast, reaching a certain negative minimum whose value is below 0 (except for $Q = 0$) and from this point relaxing to 0. The second type of curves (for PHT) does not pass through a minimum and relax to 0 but is always in the positive range. Results for IND are given by $\Delta n^*(t) = (\Delta n^*(t)_{PHT} + (e^{-Q\pi^2}\Delta n^*(t)_{PHH}))/(1 + e^{-Q\pi^2})$, which means curves with a faster relaxation than those of PHT but with no minimum and values above 0. The explanation of the

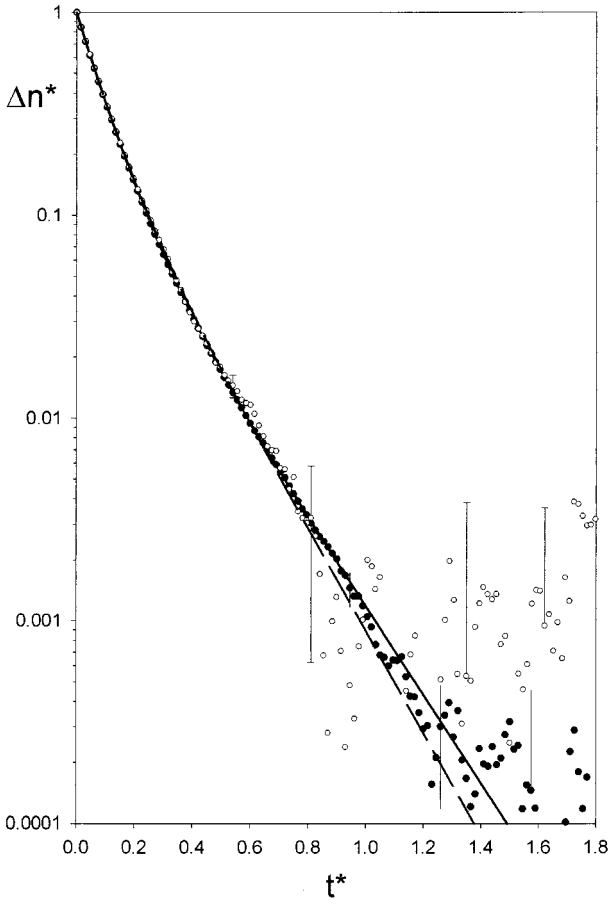

Figure 2. Birefringence decay for low and very high orienting field. Induced dipole with $Q = 0$ and no hydrodynamic interaction. Values are normalized to $n(0)$ (see eq 5). Empty circles, error bars with cap: $b = 0.5$. Filled circles, error bars with no cap: saturation ($b \rightarrow \infty$).

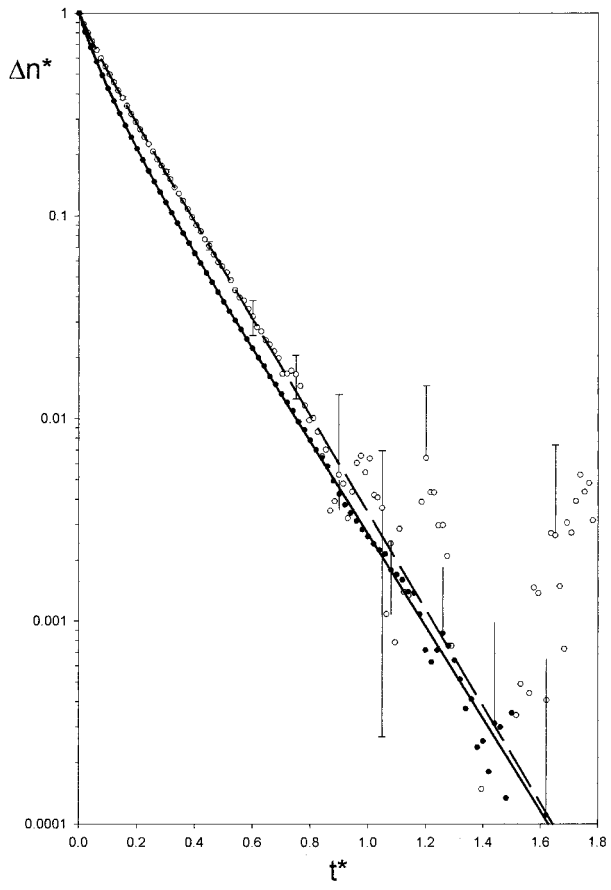

Figure 3. Birefringence decay for low and very high orienting field. Permanent head-to-tail dipole with $Q = 0$ and no hydrodynamic interaction. Values are normalized to $n(0)$ (see eq 5). Empty circles, error bars with cap: $a^2 = 1$. Filled circles, error bars with no cap: saturation ($a^2 \rightarrow \infty$).

curves for PHH dipole in terms of the orientation of the molecules is as follows. Initially all molecules are bent, with the arms aligned in the direction of the field ($\alpha = \pi$). The molecules store a very high energy equal to $kTQ\pi^2$. When the field is removed, molecules tend immediately to open but with no rotation (keeping the direction of the bisector of the arms) to the fully open conformation ($\alpha = 0$), having relaxed all the mechanical energy. They tend to be perpendicular to the field and they are closer to the totally perpendicular orientation when Q is higher, for which $\Delta n^* \approx -0.5$, according to eq 4. From this moment, the main effect is the typical rotational diffusion relaxing the value of the birefringence to 0. This characteristic behavior is observed in different degrees, depending on the intensity of the field and the flexibility of the model. Given the shape of the PHH curves, some amplitudes should be negative, which increases the intrinsic difficulties associated with the procedure of fitting. This "birefringence sign reversal" has been observed previously in the study of DNA in strong electric fields.[21,22]

Decay profiles for permanent dipoles (PHT) do depend on field strengths; this dependence is not observed for induced dipoles. When the field is weak, in PHT curves the amplitude (a_1) corresponding to the longest relaxation time (τ_1) takes a value close to unity and the appearance of the curve is practically monoexponential, but when the field is very high a clear multiexponential behavior can be observed (in fact, three exponentials can be detected) and a much lower value for a_1 is obtained (Figure 3 and Table 1). In studying intermediate situations (results not shown), a clear tendency to the limiting values given by the $E \rightarrow \infty$ case can be observed. For IND, no difference in the decay curves is observed (Figure 2). These results agree with those shown by Zacharias and Hagerman,[28] assuming their interpretation that their results are valid only for the induced dipole case or where the influence of permanent dipoles on orientation is small. The different behavior shown by the two orientation mechanisms could be exploited in experimental studies.

The decay profiles are not independent of the orienting mechanism for relatively low fields. According to the results presented in Tables 1 and 2, only for intermediate or high values of Q and strong fields do both orienting mechanisms yield the same results. We think that this behavior should be taken into account when interpreting the results presented by Allison and Nambi[25] for a saturation-induced dipole orienting mechanism which were coincident with the ones for the purely induced dipole. At the same time, our conclusion should limit the assumption made in the work by Zacharias and Hagerman[28] to study the birefringence decay profile of RNA helices. On the other hand, Wegener[23] presented an analytical treatment for rigid bodies at low field strengths in which the decay profiles depended not only on the orienting mechanism but also on the time that the field was applied.

Given the same model (identical flexibility), the longest relaxation time is the same for any intensity of the field and any orientation mechanism. Of course, its value depends on the value of Q and on the inclusion of hydrodynamic interaction. Moreover, although we must keep in mind that for PHT and low field some exponentials are not detected, it seems plausible

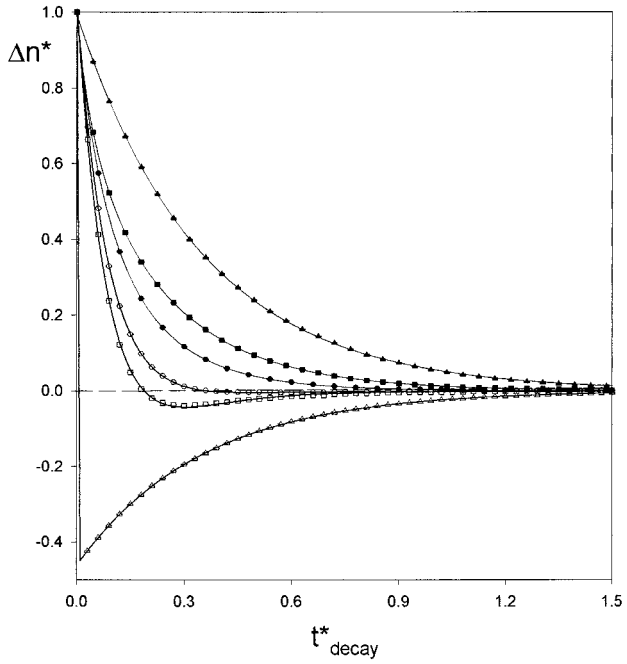

Figure 4. Birefringence decay from saturation conditions for different flexibilities of permanent head-to-tail and head-to-head dipoles. Simulations performed without hydrodynamic interaction. Circles: $Q = 0$. Squares: $Q = 0.5$. Triangles: $Q = 50$. Filled symbols: permanent head-to-tail dipole. Empty symbols: permanent head-to-head dipole.

to think that this is due to the lack of a detectable value of the amplitudes more than a change in the time spectrum. As a consequence, we could conclude that the characteristic time constants do not depend on the type of dipole or the intensity of the field. This idea should extent to flexible models the one applied for rigid bodies in which, for a molecule, its relaxation times just depend on its internal characteristics defined through its rotational diffusion tensor.[6,23]

Amplitudes depend on the type of dipole and, for PHT (not IND), on the intensity of the field. In his study of rigid bent rods, Wegener[23] found that the relative amplitudes of the birefringence decay profiles were dependent on the orienting mechanism (pure or mixed dipole character) and on the time the field was applied. Our results are obtained for flexible models, which relax after the steady state has been reached. Both treatments coincide in the idea that the orienting mechanisms and conditions applied up to the instant in which the decay starts are reflected in the preexponential factors, but not in the relaxation times.

When hydrodynamic interaction is included in the simulations, former conclusions are also applicable. The main effect of including this interaction is that the relaxation process is slower and, therefore, relaxation times are higher. As expected, the effect is more remarkable for higher flexibility, ranging from increases (in τ_1) around 25% for $Q = 50$ to 90% for $Q = 0$ (to enlarge the effect, hydrodynamic radius of the spheres has been set to a maximum of touching spheres). We must mention here the low statistical quality of the data when hydrodynamic interaction is included, which forced us to increase around eight times the number of steps to obtain results with reproducibility comparable to the ones obtained without taking into account this effect.

Amplitudes do not depend on hydrodynamic interaction. According to Tables 1 and 2, results with and without the inclusion of this effect are the same within statistical uncertainties for all the cases studied. From a theoretical point of view, this is a very interesting conclusion. In fact, some simplified or approximated theories, which are able to predict amplitudes, could be correctly applied to the interpretation of experimental results (see, for example, ref 24). We do not have knowledge of any previous work in which this result has been obtained explicitly.

Initial time, τ_{ini}, depends on field strength and hydrodynamic interaction, but when the field is very high, τ_{ini} does not depend on the flexibility of the model or nature of the dipole. To obtain this parameter with the maximum precision, we have performed series of simulations just for the initial part of the decay, enlarging the density of points in that area. Typically we simulated 20 Brownian steps of $\Delta t^* = 1 \times 10^{-4}$ for 10 000 molecules. With the points calculated, arranged in the form ln $y(t)$ versus t^*, we obtain a polynomial fitting of order 3. The lineal coefficient, according to eq 9, is $-1/\tau_{\mathrm{ini}}$. As can be seen in Tables 1 and 2, results show that this initial decay depends on the hydrodynamic interaction and the intensity of the field. For very strong fields the values obtained show no dependence on the flexibility of the model or nature of the dipole, and we can obtain averages for all models with no HI $\tau_{\mathrm{ini}} = 0.079 \pm 0.002$ and with hydrodynamic interaction $\tau_{\mathrm{ini}} = 0.143 \pm 0.004$. These values show that τ_{ini} with no HI is the same value (0.08) given by the Harvey−Wegener treatment (see ref 29). The consequence of hydrodynamic interaction is very clear, with an increase close to 100% in the initial relaxation time; that means a much slower dynamic when this effect is considered. Another significant point is the difference from the Roitman−Zimm results. It is very likely that the discrepancies are consequences of differences in the model, given, in their case, by perfectly rigid connectors and perfectly stiff straight conformation in the rigid limit. On the other hand, the other characteristic relaxation time, τ_{mean}, is very sensitive to the type of dipole, but results are not really conclusive.

Results from Roitman and Zimm[24,41] obtained for an induced dipole are valid (as long as HI is neglected) for any field strength, despite that those authors take as an initial approximation a low orientation field situation. Comparison of our IND simulation calculations with the Roitman−Zimm values show differences, in both amplitudes and relaxation times, which are between 5% and 10% (lower values for amplitudes and higher for times in those obtained from simulations).

Acknowledgment. This work has been funded by Grants PB96-1106 from Dirección General de Investigación Científica y Técnica (Ministerio de Educación y Cultura) and 01758/CV/98 from Fundación Séneca (Comunidad Autónoma de la Región de Murcia). B.C. is supported by a postdoctoral fellowship from CajaMurcia.

References and Notes

(1) Frederick, E.; Houssier, C. *Electric Dichroism and Electric Birefringence*; Clarendon Press: Oxford, 1973.

(2) O'Konski, Ch., Ed.; *Molecular Electrooptics, Part 1−Theory and Methods*; Marcel Dekker: New York, 1976.

(3) Krause, S., Ed.; *Molecular electro-Optics*; Plenum Press: New York, 1981.

(4) Riande, E.; Saiz, E. *Dipole Moments and Birefringence of Polymers*; Prentice Hall: Englewood Cliffs, NJ, 1992.

(5) Wegener, R. M.; Dowben, R. M.; Koester, V. J. *J. Chem. Phys.* **1979**, *70*, 622.

(6) García de la Torre, J.; Bloomfield, V. *Q. Rev. Biophys.* **1981**, *14*, 81.

(7) Bloomfield V. A.; Crothers D. M.; Tinoco, I. *Physical chemistry of nucleic acids*; Harper and Row: New York, 1974.

(8) Hagerman, P. J. *Biopolymers* **1982**, *20*, 1503.

(9) Nickol, J.; Rau, D. *J. Mol. Biol.* **1992**, *228*, 115.

(10) Mills, J. B.; Vacano, E.; Hagerman, P. J. *J. Mol. Biol.* **1999**, *285*, 245.
(11) Yguerabide, J.; Epstein, H. F.; Stryer, L. *J. Mol. Biol.* **1970**, *51*, 573.
(12) Carrasco, B.; Díaz, F. G., López Martínez, M. C.; García de la Torre, J. J. *Phys. Chem*. **1999**, *103*, 7822.
(13) Bernengo, J. C.; Cardinaud, R. *J. Mol. Biol.* **1982**, *159*, 501.
(14) Curry, J. F.; Krause, S. *Biopolymers* **1991**, *31*, 1677.
(15) Cardinaud, R.; Bernengo, J. C. *Biophys. J.* **1985**, *48*, 751.
(16) Holcomb, D. N.; Tinoco, I. J. *J. Phys. Chem.* **1963**, *67*, 2691.
(17) Pérez Belmonte, A.; López Martínez, M. C.; García de la Torre, J. *J. Phys. Chem.* **1991**, *95*, 952.
(18) Pérez Belmonte, A.; López Martínez, M. C.; García de la Torre, J. *J. Phys. Chem.* **1991**, *95*, 5661.
(19) Carrasco Gómez, B.; Pérez Belmonte, A.; López Martínez, M. C.; García de la Torre, J. *J. Phys. Chem.* **1996**, *100*, 9900.
(20) Antosiewicz, J.; Pörschke, D. *Biophys. Chem.* **1989**, *33*, 19.
(21) Elvingston, C. *Chem. Phys. Lett.* **1993**, *214*, 91.
(22) Mazur, S.; Allison, S. A. *J. Phys. Chem.* **1997**, *101*, 22244.
(23) Wegener, R. M. *J. Chem. Phys.* **1986**, *84*, 5989.
(24) Roitman, D. B.; Zimm, B. H. *J. Chem. Phys.* **1984**, *81*, 6348.
(25) Allison, S. A.; Nambi, P. *Macromolecules* **1992**, *25*, 759.
(26) Eden, D.; Highsmith, S. *Biophys. J.* **1997**, *73*, 952.
(27) Vacano, E.; Hagerman, P. J. *Biophys. J.* **1997**, *73*, 306.
(28) Zacharias, M.; Hagerman, P. *Biophys. J.* **1997**, *73*, 318.
(29) García de la Torre, J. *Eur. Biophys. J.* **1994**, *23*, 307.
(30) Díaz, F. G.; García de la Torre, J.; Freire, J. J. *Macromolecules* **1990**, *23*, 3144.
(31) López Cascales, J. J.; Navarro, S.; García de la Torre, J. *Macromolecules* **1992**, *25*, 3574.
(32) López Cascales, J. J.; Díaz, F. G.; García de la Torre, J. *Polymer* **1995**, *36*, 345.
(33) Bowers, J. S.; Prud'homme, R. K. *J. Chem. Phys.* **1992**, *96*, 7135.
(34) Blake Golf, R.; Karel, S. F.; Prud'homme, R. K. *J. Chem. Phys.* **1994**, *100*, 2289.
(35) Díaz, F. G.; García de la Torre, J. *J. Chem. Phys.* **1988**, *88*, 7698.
(36) Díaz, F. G.; Iniesta, A.; García de la Torre, J. *Biopolymers* **1990**, *29*, 547.
(37) Díaz, F. G.; López Cascales, J. J.; García de la Torre, J. *J. Biochem. Biophys. Methods* **1993**, *26*, 261.
(38) Díaz, F. G.; García de la Torre, J. *Macromolecules* **1994**, *27*, 5371.
(39) Lewis, R. G.; Allison, S. A.; Eden, D.; Pecora, R. *J. Chem. Phys.* **1988**, *89*, 2490.
(40) Hassager, O. *J. Chem. Phys.* **1974**, *60*, 2111.
(41) Roitman, D. B.; Zimm, B. H. *J. Chem. Phys.* **1984**, *81*, 6356.
(42) Ermak, D. L.; McCammon, J. A. *J. Chem. Phys.* **1978**, *69*, 1352.
(43) Iniesta, A.; Garcia de la Torre, J. *J. Chem. Phys.* **1990**, *92*, 2015.
(44) Rotne, J.; Prager, J. *J. Chem. Phys.* **1969**, *50*, 4831.
(45) Yamakawa, H. *J. Chem. Phys.* **1970**, *53*, 436.
(46) *Sigmaplot for Windows*, version 4.00; SPSS Inc., 1997.
(47) Provencher, S. *J. Chem Phys.* **1976**, *64*, 2272.
(48) Provencher, S. *Biophys. J.* **1976**, *16*, 27.
(49) Navarro, S.; López Martínez, M. C.; García de la Torre, J. *J. Chem. Phys.* **1995**, *103*, 7631.